Monopole Antennas for Microwave Catheter Ablation

Sylvain Labonté, *Member, IEEE,* Angeline Blais, *Student Member, IEEE,* Stéphane R. Legault, *Student Member, IEEE,* Hassan O. Ali, and Langis Roy, *Member, IEEE*

Abstract— **We study the characteristics of various monopole antennas for microwave catheter ablation of the endocardium. The investigation is done with a computer model based on the finite-element method in the frequency domain. Three monopole geometries are considered: open-tip, dielectric-tip, and metal-tip. Calculations are made for the magnetic field, the reflection coefficient and the power deposition pattern of the antennas immersed in normal saline. The theoretical results are compared with measurements performed on prototypes and good agreement is obtained. The antenna characteristics suggest that the metal-tip monopole best fulfills the requirements of catheter ablation. The computer model is then used to compare metal-tip monopoles of different dimensions and to determine design trade-offs.**

I. Introduction

RADIO-FREQUENCY (RF) catheter ablation is a medical procedure introduced in the mid-1980s for the treatment of cardiac arrhythmias. It involves burning the site of the arrhythmia—located inside the heart—with the application of electrical energy at frequencies of 0.5–1 MHz. The energy is delivered by electrodes at the end of a catheter which is advanced into the heart through one of the great blood vessels. The catheter is also used to record the electrograms needed to locate the arrhythmogenic site. The treatment is much less traumatic than open heart surgery and is usually completed within one hour.

Radio-frequency ablation relies on the flow of current between the catheter electrode and a large plate electrode on the skin of the patient to produce a lesion by Joule heating [1]. The resulting lesions are small but relatively deep. The technique has had great success in the treatment of supra-ventricular arrhythmias. However, in cases where the site to be destroyed is large and shallow or covered by insulating tissues (such as ventricular tachycardias), RF ablation is ineffective [2].

The use of microwave energy has been considered as a way to achieve larger lesions because its radiant nature allows penetration through layers of insulating tissues. Although promising, the results reported so far on microwave ablation are inconclusive. Wonnell *et al.* [3] experimented with a helical antenna operating at 2.45 GHz and found that the volume heated by microwave ablation can be several times larger than with RF ablation. However, their antenna seems too large for practical use (length 9.5 mm, diameter 3.24 mm) and is relatively complex to fabricate. A simpler alternative is to use a monopole antenna made by stripping the outer conductor at the end of a coaxial cable [4]. Rosenbaum *et al.*, used such monopoles for microwave ablation on in-vitro and in-vivo models [5] and concluded that the lesions produced are no larger than those created by RF catheters. However, their study provided few details about the geometry of the monopoles and included no theoretical analysis to substantiate the experimental findings.

Microwave antennas have been used for many years in interstitial hyperthermia, a different type of treatment. There, the antenna is inserted into a teflon catheter embedded in the tumor, thereby preventing direct electrical contact with the tissue. Many studies have been published on insulated antennas of various geometries: symmetric dipoles [6], [7], asymmetric dipoles [8], multisection dipoles [9], [10], and monopoles [11]. None of the resulting designs is directly applicable to catheter ablation of the endocardium due to their large size. An analytical study of a bare monopole in lossy medium was published recently, but was limited to electrically short antennas which did not permit an optimization of the antenna dimensions [12].

This paper presents a comparative study of monopole antennas of various geometries for use in microwave ablation and extends the analysis to identify design trade-offs. The special requirements of this application are that the antennas: 1) be small; 2) conform well to the catheter for easy catheterization; 3) possess exposed metallic parts to record electrograms of the heart; 4) present low return loss to avoid excessive heating of the coaxial feed-line; and 5) produce a uniform heating pattern.

The work is divided into three parts. Section II describes the frequency-domain finite-element analysis of a generic monopole structure and the experimental procedure used for its validation. Then, in Section III we study and compare the three monopole geometries shown in Fig. 1: 1) the open-tip monopole (OTM) where the extremity of the inner conductor is in contact with the ambient medium; 2) the dielectric-tip monopole (DTM) which is completely enclosed by the dielectric; and 3) the metal-tip monopole (MTM) which provides increased electrical contact with the tissue. Numerical calculations for the reflection coefficient and the heating pattern of the antennas are presented. Since the results suggest that the MTM offers the best compromise for catheter ablation, in Section IV we focus our attention on this antenna geometry.

Manuscript received September 2, 1995; revised January 23, 1996. This work was supported in part by the Natural Sciences and Engineering Research Council of Canada.

The authors are with the Department of Electrical Engineering, University of Ottawa, Ottawa, Ontario, Canada.

Publisher Item Identifier S 0018-9480(96)07029-9.

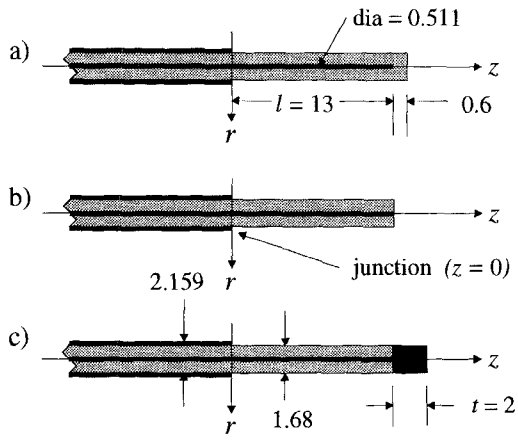

Fig. 1. Monopole antennas: (a) dielectric tip monopole (DTM), (b) open-tip monopole (OTM), and (c) metal tip monopole. Dimensions are in mm.

Simulations are carried out to highlight the design parameters affecting its performance.

Throughout this study, experimental measurements are performed to substantiate the theoretical findings. For simplicity, no attempt is made to reproduce all the conditions of catheter ablation; rather, the aim is to determine the performance of monopoles in lossy materials as a means of providing insight into the microwave ablation problem.

II. Materials and Methods

A. Finite-Element Modeling

The finite-element method (FEM) is employed because of its ability to handle complex geometries as well as material inhomogeneities. This approach is more versatile than the one adopted in [12] which is limited to short antennas. The formulation used here is based on [13] and includes higher-order modes both in the coaxial line feed and in the radiated medium.

The antennas are assumed to be immersed in a homogeneous medium so that axial symmetry obtains ($\partial/\partial\phi = 0$) and the problem reduces to 2 dimensions. In cylindrical coordinates, the modes of propagation are TM to z, and the only existing field components are E_r, E_z, and H_ϕ. Eliminating the electric field from Maxwell's curl equations we obtain the following expression for H_ϕ:

$$-\frac{\partial}{\partial z}\left(\frac{\partial H_\phi}{\partial z}\right) - \frac{\partial}{\partial r}\left[\frac{1}{r}\frac{\partial}{\partial r}(rH_\phi)\right] = \omega^2\mu\epsilon H_\phi \qquad (1)$$

where $\epsilon = \epsilon_0\epsilon_r - j\sigma/\omega$.

The FEM is used to solve the above equation with a trial solution for H_ϕ over one triangular finite element given by

$$H_\phi \approx \sum_{j=1}^{3} u_j N_j(r, z) \qquad (2)$$

where u_j are unknown complex constants and $N_j(r, z)$ are real-valued, first-order interpolatory functions. Following Galerkin's procedure, (1) is transformed into a set of linear algebraic equations. Over one finite element, this equation can be cast in the following form:

$$\sum_{j=1}^{3} u_j \iint Y\left(\frac{\partial N_i}{\partial r}\frac{\partial N_j}{\partial r} + \frac{\partial N_i}{\partial z}\frac{\partial N_j}{\partial z} + \frac{1}{r}N_j\frac{\partial N_i}{\partial r}\right) + ZN_iN_j\,dr\,dz = \oint E_tN_i\,dl \quad i = 1, 2, 3 \qquad (3)$$

where $Y = (\sigma + j\omega)^{-1}$, $Z = j\omega\mu$ and E_t is the tangential counterclockwise component of the elemental boundary electric field. The H_ϕ formulation is preferred over the rH_ϕ formulation introduced in [14] because of the ability to work around the singularity associated with the surface integrals of (3). In addition, it gives rise to considerably fewer and simpler integrals requiring analytical solution.

The elemental systems are assembled in the usual FEM fashion to produce a sparse matrix equation for H_ϕ. The boundary conditions associated with the problem are introduced as follows:

1) Along the z-axis (Fig. 2), $H_\phi = 0$ because of symmetry. This permits complete elimination of the unknowns associated with nodes falling on the axis of symmetry, thereby reducing the order of the matrix equation.
2) On the inner and outer conductors of the coaxial cable which are assumed perfectly conducting, the tangential E-field is zero. Accordingly, nodes on those boundaries have no contribution on the right-hand side vector.
3) A TEM radiation condition is enforced on the outer spherical boundary [14]. In our case, the location of this boundary is not critical, because the radiated field is rapidly dissipated in the surrounding lossy medium. Experience shows that below 5 GHz, the results do not depend on the boundary location when it is at $r \geq 40$ mm.
4) In the feeding coaxial cable at a point sufficiently far from the junction, a TEM mode is assumed. The total magnetic field (H_ϕ) is the difference between the incident wave (H_ϕ^+) and the reflected wave (H_ϕ^-). At the feed plane, the FEM formulation must allow for the application of a known incident wave, and simultaneously present a reflectionless termination for the unknown reflected wave. This is made possible by expressing H_ϕ^- as $(H_\phi^+ - H_\phi)$ and by writing a Neumann boundary condition for H_ϕ as follows:

$$\frac{\partial H_\phi}{\partial z} = -jk(2H_\phi^+ - H_\phi). \qquad (4)$$

where k is the propagation constant in the coaxial cable. Equation (4) is used to specify the excitation at the feed plane.

More details about the boundary conditions for this FEM formulation can be found in [13].

Once $H_\phi(r, z)$ is calculated, it can be decomposed into incident and reflected waves at the feed-boundary. This information is used to calculate the voltage reflection coefficient of the antenna.

In the ambient medium, the E-field is derived from

$$E_r = \frac{-1}{j\omega\epsilon}\frac{\partial H_\phi}{\partial z} \qquad (5)$$

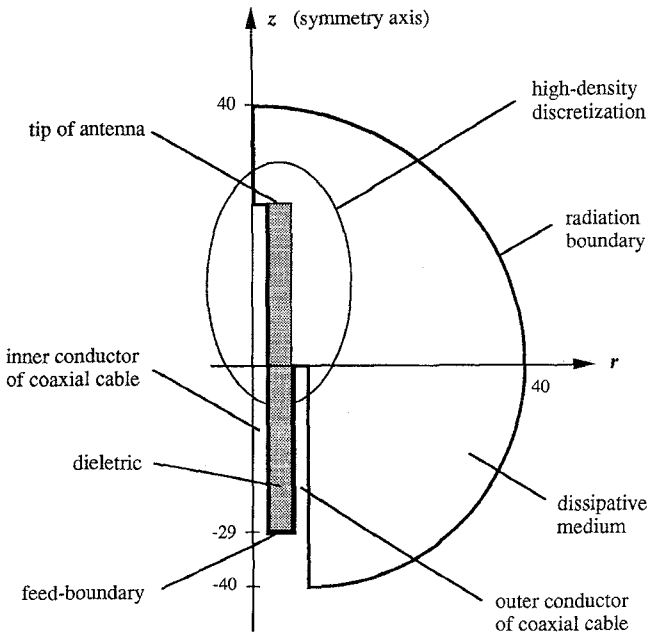

Fig. 2. Solution domain of FEM computation. The open-tip monopole is shown. Inside the cable dielectric and in the region of high density discretization, triangle size is roughly 0.1 mm. Drawing is not to scale.

and

$$E_z = \frac{1}{j\omega\epsilon}\left(\frac{1}{r}\frac{\partial}{\partial r} rH_\phi\right) \tag{6}$$

using finite-difference approximations. Finally, the specific absorption rate (SAR) (W m^{-3}) is obtained with

$$\text{SAR} = \frac{\sigma}{2}(|E_r|^2 + |E_z|^2). \tag{7}$$

In this analysis the feed-boundary is located at $z = -29$ mm which ensures that higher-order modes reflected by the antenna junction have decayed to insignificant magnitudes [15]. Convergence tests have revealed that roughly 10 000 triangular elements are needed to provide an acceptable solution.

Although in a real application the antennas would be used to ablate heart tissue, all simulations are done with the antennas surrounded by normal saline (0.9%) at room temperature. This is to overcome the difficulty of modeling cardiac tissues whose electrical properties are not accurately known and vary considerably between individuals. Conversely, saline is well characterized with properties at 2.45 GHz comparable to those of average heart tissue. The accurate characterization of saline facilitates validation of the model by comparing the calculated and measured reflection coefficient of various antennas over a wide frequency range. The frequency dependent electrical properties of saline are taken from the literature [16].

B. Experimentation

To verify the numerical results, the reflection coefficient and the temperature distribution of a number of antenna prototypes are measured. These prototypes are made by stripping the outer conductor of a 0.085 in (2.159 mm) 50-Ω semirigid coaxial cable (Fig. 1). The metal-tip is fabricated with a short section of 1/16 in (1.59 mm) brass tubing, soldered to the inner conductor. The dielectric tip is obtained by retracting the center conductor and filling the vacated space with Vaseline which has dielectric properties similar to teflon [17]. The prototypes are equipped with SMA connectors and have an overall length of 15 cm.

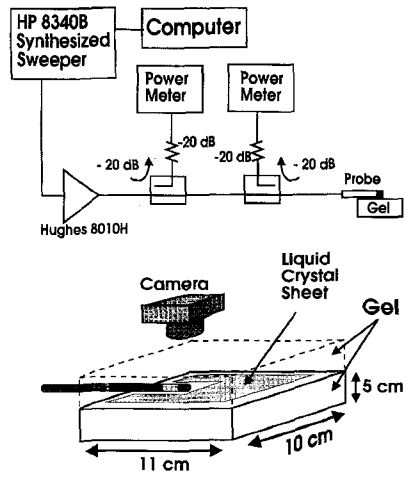

Fig. 3. Experimental setup and details of the split-block experiment.

TABLE I
DIELECTRIC CONSTANT AND CONDUCTIVITY AT ROOM TEMPERATURE AND AT 2.45 GHZ. THE PROPERTIES OF HEART ARE FROM [22]. FREQUENCY-DEPENDENT PROPERTIES OF SALINE CAN BE OBTAINED FROM [16]

	average heart	9ppt saline	gel
ϵ	47	75	69 ± 5%
σ [S m^{-1}]	2.17	2.81	2.86 ± 5%

For measuring the reflection coefficient we use a calibrated network analyzer (HP8510). The measurements are done with the antennas immersed in normal saline at room temperature. In order to remove any artifact due to the saline-air interface, the antennas are positioned vertically at least 35 mm below the surface.

The temperature distribution around the antennas is obtained by the split-block technique and a liquid crystal sheet (LCS). This approach consists in placing a LCS and the antenna under test between two blocks of gel as shown in Fig. 3. Following the application of microwave power to the antenna, the two blocks are separated and the temperature distribution recorded on the LCS is photographed. The gel, specially developed for this work, is prepared by mixing 90.14% H_2O, 0.76% NaCl, and 9.01% HEC (Hydroxy ethyl cellulose, a gelling agent) to achieve the desired properties, as indicated in Table I. The resulting product is very firm, yellowish, and transparent. This last property turns out to be very convenient with the split-block technique because it allows the operator to verify visually the proper placement of the antenna and the LCS between the gel blocks. The addition of bacteriacide (0.09%) to the gel allows for the preservation of its properties for weeks at room temperature. The gel properties are measured with an open-ended coaxial probe [18] and are found to be reproducible within a few percent.

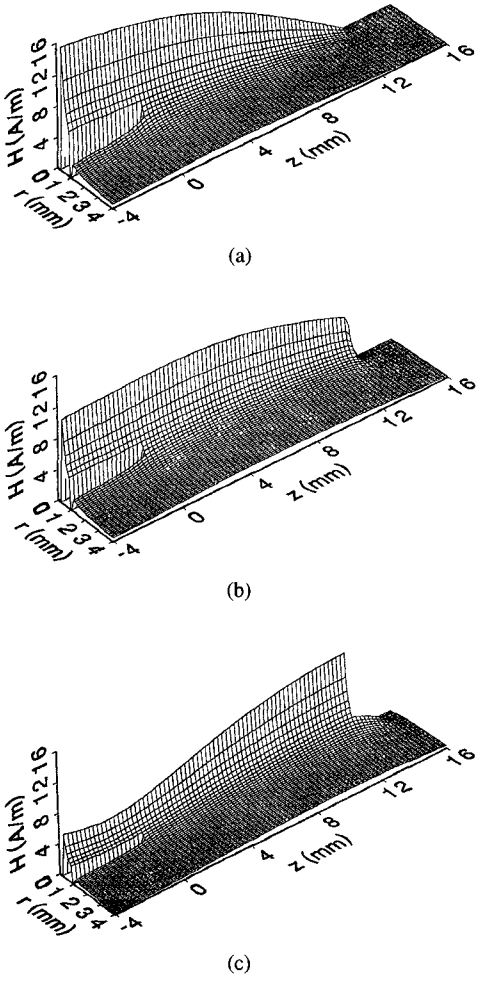

Fig. 4. Magnitude of H_ϕ around the monopoles. The inner and outer conductors of the coaxial cable are at $r = 0$ and $r = 0.84$ mm, respectively. (a) DTM, (b) OTM, and (c) MTM.

Liquid crystal sheets are inexpensive and easy to handle. They offer a high spatial resolution at the expense of a relatively low absolute thermal accuracy. In this work the use of LCS is adequate because we are interested in the comparison of various antennas and absolute accuracy is not essential. The LCS we selected is type S72,374 from Edmund Scientific, Barrington, NJ, with a temperature range of 25–30°C. It is thin enough (0.14 mm) that its presence between the two gel blocks has no noticeable effect on the reflection coefficient of the antennas. To ensure meaningful comparisons, the same liquid crystal sheet is used to characterize all antennas. In addition, tests have been conducted to confirm the reproducibility of the color patterns of the LCS.

A synthesizer (HP8340B) and an amplifier (Hughes 8010H) are used to supply microwave energy to the antennas with the incident and reflected power monitored to ensure proper operation (Fig. 3). The optimum level and duration of heating was determined in order to achieve clear color patterns on the LCS and to minimize cooling time between experiments. We found that a total power dissipation of about 13 W for 12 s was adequate with a resulting color pattern stable enough to allow a picture to be taken. Under these experimental conditions, the reflection coefficient did not change significantly during

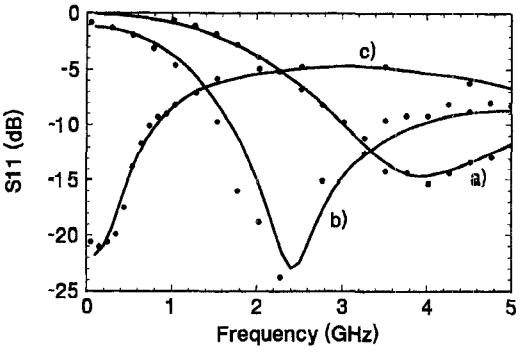

Fig. 5. Reflection coefficients for: a) the DTM; b) the OTM; and c) the MTM. The continuous curves are calculated, the discrete points are experimental.

heating. For meaningful comparison, the various antennas were all tested with the same total dissipated power (within the ranges of the variability in the amplifier output level after on/off switching). This power was calculated taking into account the loss in the cables and the reflection coefficient of the antennas.

To confirm the adequacy of the experimental procedures at least two units of each prototype were fabricated and tested many times in different gel blocks. The results obtained exhibited very good consistency.

III. Modeling of Monopoles

A. Results

In order to better understand the differences between possible monopole geometries, the three monopoles of Fig. 1 are simulated.

Fig. 4 displays the magnitude of H_ϕ calculated inside the dielectric and around the antennas for an input voltage of 1 V (peak) at 2.45 GHz. On the DTM the field is zero at the tip and increases toward the junction ($z = 0$). The field is much more uniform on the OTM but nonetheless decreases toward the tip. The MTM displays a minimum of the field at the junction and a maximum near the tip.

In Fig. 5, the reflection coefficient of the antennas are presented as a function of frequency. Good agreement is obtained over a wide frequency range between the calculated and measured values, validating the theoretical model. The 13 mm OTM is very well matched ($S_{11} < -20$ dB) around 2.45 GHz. The MTM is well matched at low frequencies but at 2.45 GHz S_{11} is only -5 dB. The curve for the DTM presents a wide minimum at 4 GHz comparable to that measured on other insulated antennas [9].

Calculated SAR patterns at 2.45 GHz are plotted in Fig. 6 for the three antennas. The curves show the longitudinal variation of the SAR at $r = 1.5$ mm and are divided by $(1 - |S_{11}|^2)$ so that the total dissipated power is the same in all cases. The plot reveals that the SAR distributions differ significantly from one antenna to another. The DTM has a highly concentrated SAR near the junction and almost none at the tip. The MTM has a more uniform distribution with a

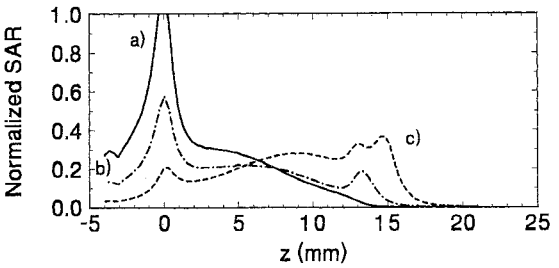

Fig. 6. Calculated SAR patterns at $r = 1.5$ mm for: a) DTM; b) OTM; and c) MTM. The curves are all divided by $(1 - |S_{11}|^2)$ and normalized to 30 kW m^{-3}. Curve a) peaks at 1.13.

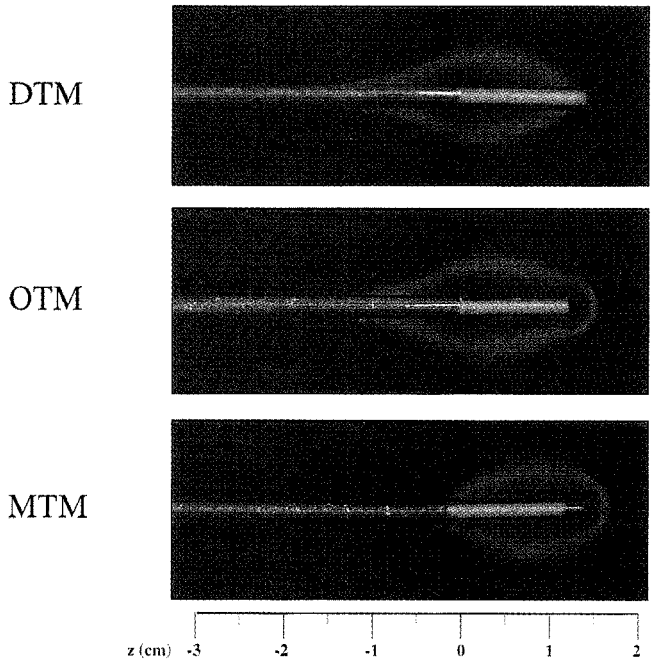

Fig. 7. Temperature distribution produced in gel after 12 s of power application. The power dissipated was constant at 13.4 W for the DTM, 13.4 W for the OTM, and 11.8 W for the MTM.

wide maximum around the tip. The OTM displays intermediate characteristics.

Fig. 7 shows the temperature patterns recorded in the gel. The blue, green, red, and black color sequence indicates decreasing temperature. In the 3 cases, power was applied for 12 s and was 13.4 W for the DTM, 13.4 W for the OTM, and 11.8 W for the MTM. The temperature distribution shown here is not the same as the SAR distribution but gives a good indication of where the hot spots are located. As previously observed in Fig. 6, little heating occurs at the tip of the DTM compared to the other antennas. The shapes of the isotherms clearly indicate that the DTM has a hot spot at the junction, the OTM has one at the tip and at one the junction, while the MTM has uniform heating. These observations all agree with Fig. 6.

B. Discussion

It is instructive to interpret the magnetic field plots of Fig. 4 on the basis of the quasi-static approximation. Under this

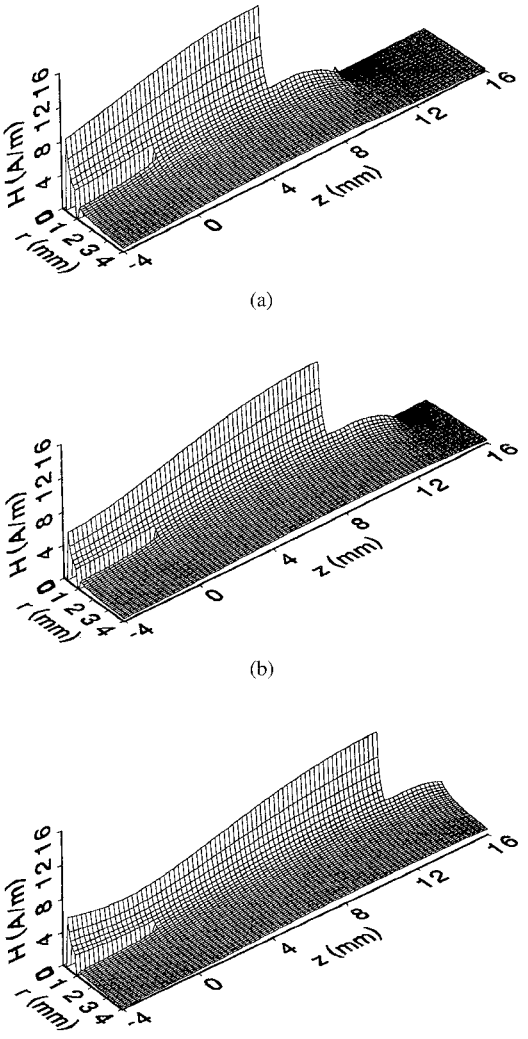

Fig. 8. H_ϕ for 3 metal-tip monopoles in 0.9% saline: (a) $l = 6.5$, $t = 4$ mm; (b) $l = 10$, $t = 4$ mm; and (c) $l = 13$, $t = 4$ mm.

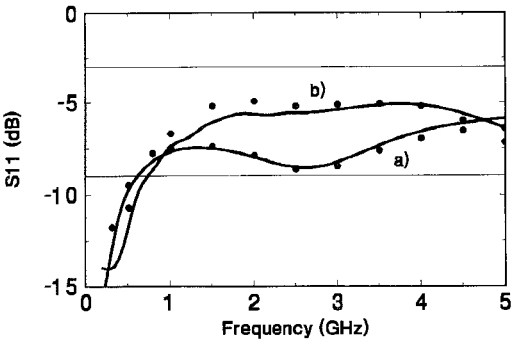

Fig. 9. Reflection coefficient for two metal-tip monopoles in 0.9% saline: (a) $l = 6.5$, $t = 4$ mm and (b) $l = 13$, $t = 4$ mm. The points are experimental values. The horizontal lines are at -3 and -9 dB.

approximation, near the antenna H_ϕ is given by $I(z)/2\pi r$ where $I(z)$ is the antenna current. Therefore the distribution of H_ϕ close to the z-axis is a good indication of the current distribution on the antenna.

In Fig. 4(a), the results show that the DTM has a current null at the tip. This agrees with the theory by King [6], which states

that insulated antennas of this type behave as lossy coaxial lines terminated in an open-circuit at the tip.

Extending King's transmission-line analogy, one predicts that the antenna current for the OTM and the MTM should be different from zero at their tip because the center conductor is in contact with the lossy ambient medium. This is confirmed by the results of Fig. 4(b) and (c), which also reveal a considerable difference between the two current distributions. For the OTM the current magnitude is constant for the first half of the monopole and drops gradually toward the tip. For the MTM the current magnitude varies along the antenna with a characteristic standing wave pattern. At the metal-tip junction ($z = 13$ mm), the total current on the inner conductor should be the same as the total current flowing on the surface of the metal-tip. This is confirmed by the continuity of the magnetic field at $z = 13$, $r = 0.84$ mm [Fig. 4(c)]. Further along the tip itself, the current drops rapidly because it spreads in the surrounding medium.

Fig. 4 also shows the current flowing on the exterior of the outer conductor of the coaxial line, near the junction. The effect of this current is seen in Fig. 7 by the extension of the heating pattern into the area $z < 0$. In interstitial microwave hyperthermia, this current is problematic because it varies with the insertion depth of the applicator. Consequently, the heating pattern and reflection coefficient of the antenna also depend on the insertion depth, which is undesirable. A sleeve balun has been proposed to eliminate this current [19]. No such problem is expected in microwave ablation because the catheter is largely inside the body and the air interface is too far to have an effect on the antenna at its tip.

The reflection coefficients at 2.45 GHz confirm the above observations on antenna currents. The OTM presents a very low return loss indicated by the constant current magnitude up to $z = 6$ mm. On the other hand, the DTM and MTM present a standing wave pattern which in the latter case is responsible for increased tip heating.

All the monopole antennas radiate predominantly laterally and hence, in order to burn the endocardium, the catheter must be placed parallel to it. This contrasts with conventional RF ablation where the catheter touches the heart more or less at right angle. However, a recent study demonstrates the feasibility and advantage of using catheters in lateral contact, especially for the treatment of ventricular tachycardias [20].

The DTM does not have an exposed metallic part near its tip, which complicates the recording of electrograms and thus catheter positioning. Furthermore, it produces a highly nonuniform heating pattern. The return loss could possibly be improved by increasing the length of the antenna but this would make it too long for practical use. The DTM is thus of limited practical interest for microwave ablation. However, it serves as a convenient means of verifying our numerical procedure and provides useful insight into the physics of the problem.

The OTM is very well matched in its current state and has a relatively uniform heating pattern. The exposed end of the inner conductor at the antenna tip can be used for electrograms, but its small size may limit its effectiveness for this purpose. On the other hand, the MTM offers a uniform heating pattern and a large exposed metallic tip but it has a fairly high reflection coefficient at 2.45 GHz (−5 dB).

Because of the ease with which electrograms can be measured, we feel that the MTM represents the best overall compromise for microwave ablation. However, the return loss of the MTM in its present form needs improvement. In the following section, we determine how the dimensions of a MTM affect its performance.

IV. Optimization of MTM

Two parameters of the antenna, the length of the exposed dielectric (l) and the length of the metallic tip (t) are varied so as to observe the effect on the S_{11} and the SAR. Simulations with $l = 6.5$, 10, 13, and 16 mm and $t = 1$, 2, and 4 mm are performed. Larger dimensions are not considered because they are impractical for catheter ablation. The results for the magnetic field, SAR, and reflection coefficients are shown in Figs. 8–11.

Plots of the magnetic field for three MTM's of various lengths ($l = 6.5$, 10, and 13 mm) and constant $t = 4$ mm are shown in Fig. 8. For conciseness, only these field results are presented although the fields obtained with the other antenna dimensions can easily be inferred from them. The magnetic field distribution varies smoothly and in a predictable manner as l increases. The plots show that the current on the exterior of the *outer* coaxial conductor ($z < 0$) is minimized for the longest antenna. This can be related to the fact that for this antenna, the *inner* conductor current is at a minimum at the junction. Fig. 8 also reveals that for all MTM's, current flows along the entire length of the metal tip.

All S_{11} results are similar and typical frequency responses are plotted in Fig. 9. Generally, for a given antenna length l, the tip length t does not affect S_{11} significantly between 1.5–3.5 GHz. The exception is $l = 6.5$, $t = 4$ mm (shown) which results in $S_{11} = -9$ dB, 2 dB less than with the other t values. At 2.45 GHz and for a given tip length t, S_{11} increases with l: by roughly 2 dB for $l = 6$ to $l = 10$ mm and 1 dB for $l = 10$ to $l = 16$ mm. The best matched monopole at 2.45 GHz is $l = 6.5$, $t = 4$ mm.

Curves of normalized SAR versus z at $r = 1.5$ mm are shown in Fig. 10 for all monopoles. The SAR patterns are characterized in all cases by three peaks caused by edge effects: one at the junction, and one at each of the two edges of the metal-tip. Depending on t, the latter two may overlap to some extent. With $t = 1$ mm, they merge and form only one peak. With $t = 4$ mm they are clearly separated. The length t of the metal tip thus has a direct influence on the uniformity of the SAR. For $l = 6.5$ and 10 mm the SAR peaks at the junction and at the tip of the antenna are of similar magnitude. For $l \geq 13$ mm, heating becomes more important at the tip than at the junction. Given this behavior, it appears that using a monopole with $l > 13$ mm is detrimental to SAR uniformity. This can be related to the antenna current which reaches a minimum at the junction for $l \approx 16$ mm (Fig. 8) and thus produces less heating at that point. The curves reveal that the most uniform SAR is obtained with $l = 13$ and $t = 2$ mm.

The radial variation of the SAR has also been studied and is presented in Fig. 11. In this respect, all antennas behave

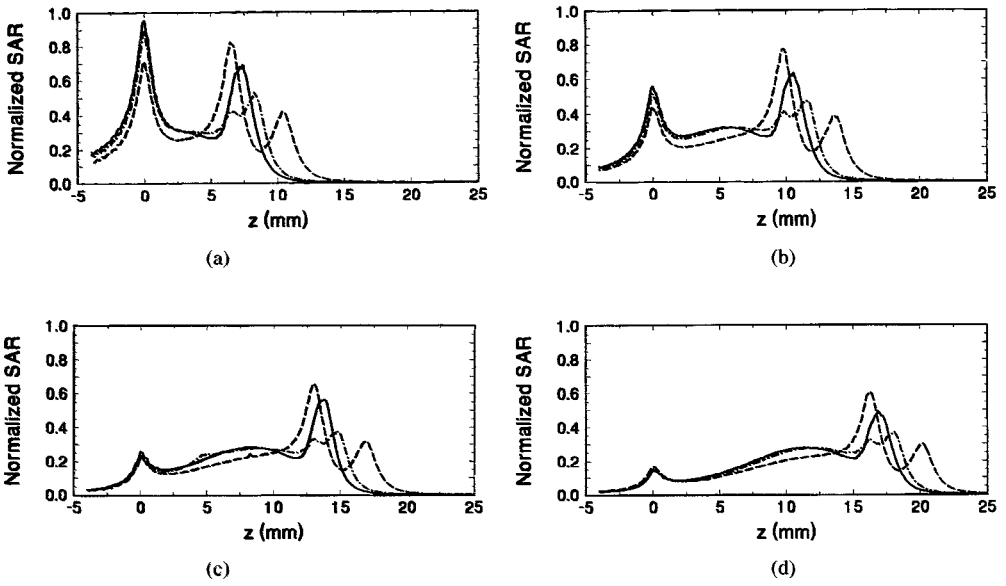

Fig. 10. Normalized SAR at $r = 1.5$ mm for all MTM's: (a) $l = 6.5$; (b) $l = 10$; (c) $l = 13$; and (d) $l = 16$ mm. In each case, the curves for $t = 1$ (solid), 2 (dot dash), and 4 mm (dash) are shown. The SAR values are divided by $(1 - |S_{11}|^2)$ and are normalized to 30 kW m^{-3}.

similarly. At the edges of the metal tip and at the junction of the antenna the SAR values are very high and decay rapidly radially as shown in curve b). At other points along the antenna where SAR values are lower, the radial rate of decrease is also lower. As shown in curve a), the SAR decreases by roughly 50% 1 mm away from the antenna surface.

As a result of this investigation, no monopole seems to satisfy all the requirements of catheter ablation. With $l = 6.5$ and $t = 4$ mm, the reflection coefficient is about -9 dB at 2.45 GHz, which is acceptable. On the other hand, the SAR is suboptimal as heating is concentrated at the junction and the edges of the tip. This may cause problems in practice because of blood and tissue coagulation at these hot spots. However, due to surface cooling during ablation [21], the thermal distribution produced in the tissue may in fact be satisfactory. In-vitro experiments appear necessary to resolve the issue. The overall length of this applicator is 10.5 mm which is adequate for catheter ablation.

The monopole with $l = 13$ and $t = 2$ mm does not present high SAR peaks and would undoubtedly produce large and uniform tissue lesions. Unfortunately, the S_{11} is fairly high at 2.45 GHz (-5 dB). This means that for a given amount of power dissipated in the tissue, more power is dissipated as heat in the catheter itself (because of inevitable losses) than with a better matched antenna. Of course, during ablation the catheter is continuously cooled by the flow of blood but it is not known at the moment if the catheter temperature would be low enough to avoid patient injury or catheter failure. The antenna has an overall length of 15 mm which seems fairly large for catheter ablation but may not be impractical. Again, more experimental work must be accomplished to clarify this question.

As a final step in the monopole study, the two antennas discussed above are measured in gel. For additional comparisons, antennas having $l = 10$, $t = 4$ and $l = 13$, $t = 4$ mm are also measured. The resulting temperature distributions after

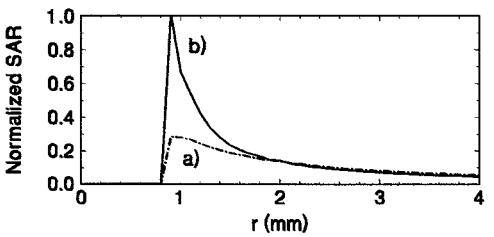

Fig. 11. SAR patterns for $l = 9$, $t = 2$ mm at: a) $z = 5$ and b) $z = 10$ mm. SAR values are divided by $(1 - |S_{11}|^2)$ and normalized to 50 kW m^{-3}.

12 s of 13 W dissipation are shown in Fig. 12. All prototypes display smooth isotherms with significant heating near the tip. The increased heating of short monopoles along the body of the cable is also evident but it is unclear whether this is a drawback for ablation.

An important feature not shown on these pictures is the fact that near the antennas, the temperature is higher for the short monopoles than the longer ones due to the higher SAR. It is well known that during RF ablation, the maximum tissue temperature must not exceed 100°C to avoid tissue coagulation [21]. When this occurs, the catheter electrode becomes covered with a layer of insulating material, effectively limiting current flow and thus lesion growth. In microwave ablation, lesion production may not be affected to the same extent by this phenomenon because the process does not rely uniquely on conduction current. Nonetheless, it is likely that for other considerations, limiting the tissue temperature to a certain maximum value would also be relevant in microwave ablation. In view of this, more power could be applied and larger lesions could be achieved with the longer antennas.

V. Conclusion

Various designs for monopole antennas were analyzed using the finite-element method. Calculations for the reflection coefficient as a function of frequency agree well with measure-

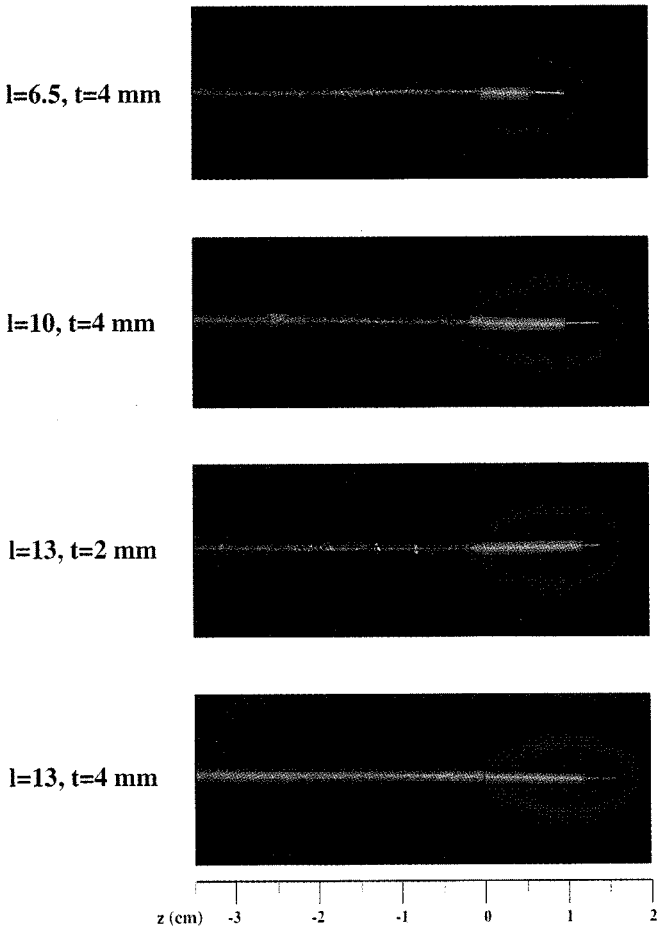

Fig. 12. Temperature distribution produced in gel after 12 s of power application for four metal-tip monopoles. The power dissipated was constant at 12.8 W for $l = 6.5$, $t = 4$ mm, 13.8 W for $l = 10$, $t = 4$ mm, 11.8 W for $l = 13$, $t = 2$ mm, and 13.5 W for $l = 13$, $t = 4$ mm.

ments performed in normal saline. The analyzes reveal that the metal-tip monopole is the best geometry as the antenna current reaches a maximum near the tip and produces a fairly uniform SAR along its length. This result is confirmed by temperature measurements in a gel developed to exhibit the same electrical properties as saline.

The optimization of metal-tip antennas undertaken here suggests that no solution yields ideal performance for ablation. The short, well matched monopole has a nonuniform SAR pattern while longer monopoles have a poorer reflection coefficient. This work cannot conclude about the best practical metal-tip monopole and we feel that in-vivo experiments are required in order to resolve the issue. However, this study does offer valuable insight into the problem which will prove useful in the interpretation of in-vivo trials.

Microwave catheter ablation with these antennas may result in improved treatment of ventricular arrhythmias. Evidently, this will require further investigation into catheter construction techniques and materials in order to adapt them to the transmission of microwave energy.

ACKNOWLEDGMENT

The authors would like to thank M.-A. Fabert and M. Lee for conducting computer simulations and fabricating the antenna prototypes. They are also grateful to Dr. A. S. L. Tang for very useful discussions about the medical aspect of catheter ablation and Dr. A. Thansandote for access to his laboratory facilities.

REFERENCES

[1] S. Labonté, "Numerical model for radio-frequency ablation of the endocardium and its experimental validation," *IEEE Trans. Biomed. Eng.*, vol. 41, no. 2, pp. 108–115, Feb. 1994.

[2] D. Newman, G. T. Evans, and M. M. Scheinman, "Catheter ablation of cardiac arrhythmias," *Curr. Probl. Cardiol.*, vol. 14, no. 3, pp. 117–164, Mar. 1989.

[3] T. L. Wonnell, P. R. Stauffer, and J. J. Langberg, "Evaluation of microwave and radio-frequency catheter ablation in a myocardium-equivalent phantom material," *IEEE Trans. Biomed. Eng.*, vol. 39, no. 10, pp. 1086–1095, Oct. 1992.

[4] L. S. Taylor, "Implantable radiators for cancer therapy by microwave hyperthermia," *Proc. IEEE*, vol. 68, no. 1, pp. 142–149, 1980.

[5] R. M. Rosenbaum, A. J. Greenspon, S. Hsu, P. Walinsky, and A. Rosen, "RF and microwave ablation for the treatment of ventricular tachycardia," in *IEEE MTT-S Dig.*, Atlanta, 1993, pp. 1155–1158.

[6] R. W. P. King, B. S. Trembly, and J. W. Strohbehn, "The electromagnetic field of an insulated antenna in a conducting or dielectric medium," *IEEE Trans. Microwave Theory Tech.*, vol. 31, no. 7, pp. 574–583, July 1983.

[7] J. P. Casey and R. Bansal, "The near field of an insulated dipole in a dissipative dielectric medium," *IEEE Trans. Microwave Theory Tech.*, vol. MTT-34, no. 4, pp. 459–463, Apr. 1986.

[8] Y. Zhang, N. V. Dubal, R. Takemoto-Hambleton, and W. T. Joines, "The determination of the electromagnetic field and SAR pattern of an interstitial applicator in a dissipative dielectric medium," *IEEE Trans. Microwave Theory Tech.*, vol. 36, no. 10, pp. 1438–1444, Oct. 1988.

[9] M. F. Iskander and A. M. Tumeh, "Design optimization of interstitial antennas," *IEEE Trans. Biomed. Eng.*, vol. 36, no. 2, pp. 238–246, Feb. 1989.

[10] A. M. Tumeh and M. F. Iskander, "Performance comparison of available interstitial antennas for microwave hyperthermia," *IEEE Trans. Microwave Theory Tech.*, vol. 37, pp. 1126–1133, July 1989.

[11] J. J. Fabre, M. Chive, L. Dubois, J. C. Camart, E. Playez, B. Prevost, L. Vanseymortier, and J. Rohart, "915 MHz microwave interstitial hyperthermia. Part 1: Theoretical and experimental aspects with temperature control by multifrequency radiometry," *Int. J. Hyperthermia*, vol. 9, no. 3, pp. 433–444, 1993.

[12] G. Cerri, R. De Leo, and V. M. Primiani, "Thermic end-fire interstitial applicator for microwave hyperthermia," *IEEE Trans. Microwave Theory Tech.*, vol. 41, nos. 6/7, pp. 1135–1142, June/July 1993.

[13] H. O. Ali and G. I. Costache, "Accurate frequency domain modeling of coaxially driven axisymmetric microwave structures," *IEEE Microwave Guided Wave Lett.*, vol. 4, no. 12, pp. 390–393, Dec. 1994.

[14] E. Sumbar, F. E. Vermeulen, and F. S. Chute, "Implementation of radiation boundary conditions in the finite element analysis of electromagnetic wave propagation," *IEEE Trans. Microwave Theory Tech.*, vol. 39, pp. 267–273, 1991.

[15] J. G. Maloney, G. S. Smith, and W. R. Scott, "Accurate computation of the radiation from simple antennas using the finite-difference time-domain method," *IEEE Trans. Antennas Propagat.*, vol. 38, pp. 1059–1068, July 1990.

[16] A. Nyshadam, C. L. Sibbald, and S. S. Stuchly, "Permittivity measurements using open-ended sensors and reference liquid calibration: An uncertainty analysis," *IEEE Trans. Microwave Theory Tech.*, vol. 40, no. 2, pp. 305–314, Feb. 1992.

[17] A. R. Von Hippel, *Dielectric Materials and Applications*. Cambridge, MA: MIT Press, 1954.

[18] M. A. Stuchly, T. W. Athey, G. M. Samaras, and G. E. Taylor, "Measurements of radio frequency permittivity of biological tissues with an open ended coaxial line: Part II—Experimental results," *IEEE Trans. Microwave Theory Tech.*, vol. MTT-30, pp. 87–92, 1982.

[19] W. Hurter, F. Reinbold, and W. J. Lorenz, "A dipole antenna for interstitial hyperthermia," *IEEE Trans. Microwave Theory Tech.*, vol. 39, no. 6, pp. 1048–1054, June 1991.

[20] M. Oeff, J. J. Langberg, M. C. Chin, W. E. Finkbeimer, and M. M. Scheinman, "Ablation of ventricular tachycardia using multiple sequential transcatheter application of radio-frequency energy," *PACE*, vol. 15, pp. 1167–1176, Aug. 1992.

[21] S. Labonté, "A computer simulation of radio-frequency ablation of the endocardium," *IEEE Trans. Biomed. Eng.*, vol. 41, no. 9, pp. 883–889,

Sept. 1994.
[22] C. K. Chou, G. W. Chen, A. W. Guy, and K. H. Luk, "Formulas for preparing phantom muscle tissue at various radio frequencies," *Bioelectromagnetics*, vol. 5, pp. 435–441, 1984.

Sylvain Labonté (S'86-M'92) was born in Sherbrooke, P.Q., Canada, in 1961. He studied electrical engineering at the University of Sherbrooke and the University of Ottawa, where he received the Ph. D. degree in 1992.

In 1988 he spent one year at the Canadian Marconi Company, Montréal, Canada as a Microwave Engineer. Between 1992 and 1996 he was an Assistant Professor of electrical engineering at the University of Ottawa and a Systems Engineer at Nortel, Ottawa, Canada. He is now a Systems Engineer with Ericsson Research, Montréal, Canada and an Adjunct Professor at the University of Ottawa. His professional interests are microwave engineering, electromagnetics, and cellular communications.

Dr. Labonté is a member of l'Ordre des Ingénieurs du Québec.

Angeline Blais (S'95) received the B.A.Sc. degree in electrical engineering from the University of Ottawa in 1994. She is now pursuing a M.A.Sc. degree at the same University.

Her main research interest is the study of electromagnetic fields and their effect on the human body.

Stéphane R. Legault (S'90) received the B.A.Sc. (E.E.) degree, summa cum laude, from the University of Ottawa in 1992 and the M.S.E E. degree from the University of Michigan in 1994. He is currently pursuing the Ph.D. degree at the University of Michigan. His research interests include various aspects of electromagnetic wave propagation and scattering.

Hassan O. Ali received the B Sc. degree in electrical engineering from the University of Dar es Salaam, Tanzania and the M.A.Sc. degree from the University of Ottawa, Ottawa, Canada. He is currently pursuing a Ph. D. degree at the same University as a Canadian Commonwealth Scholar.

From 1988 to 1990 he worked as an Assistant Lecturer at the University of Dar es Salaam, Tanzania, where he was involved in research on microwave devices especially power dividers. His main research interests are in the design of microwave and millimeter wave devices and circuits, electromagnetic interference and compatibility, and numerical modelling in electromagnetics with special interests in the finite element method. He has a number of publications in those areas.

Langis Roy (M'93) received the B.A.Sc. degree in electrical engineering fron the University of Waterloo in 1987, and the M.Eng and Ph.D. degrees from Carleton University, Ottawa, Canada, in 1989 and 1993, respectively.

In 1993 he joined the Faculty of Engineering of the University of Ottawa, where he is now a Professor of the Department of Electrical Engineering. His research interests are in GaAs monolithic microwave integrated circuits, high-efficiency microwave power amplifiers, integrated active antennas, and numerical techniques in electromagnetics.